Conductive, Capacitive, and Viscoelastic Properties of a New Composite of the C_{60}−Pd Conducting Polymer and Single-Wall Carbon Nanotubes

Piotr Pieta,[†] Emilia Grodzka,[‡] Krzysztof Winkler,[‡] Magdalena Warczak,[†] Andrzej Sadkowski,[†] Grazyna Z. Zukowska,[§] Ganesh M. Venukadasula,[||] Francis D'Souza,*[,||] and Wlodzimierz Kutner*[,†,⊥]

Institute of Physical Chemistry, Polish Academy of Sciences, Kasprzaka 44/52, 01-224 Warsaw, Poland, Institute of Chemistry, University of Bialystok, Hurtowa 1, 15-399 Białystok, Poland, Faculty of Chemistry, Warsaw University of Technology, Noakowskiego 3, 00-664 Warszawa, Poland, Department of Chemistry, Wichita State University, Wichita, Kansas 67260, and Faculty of Mathematics and Natural Sciences, School of Science, Cardinal Stefan Wyszynski University in Warsaw, Dewajtis 5, 01-815 Warsaw, Poland

Received: November 19, 2008; Revised Manuscript Received: January 29, 2009

Thin films of a new composite of an electroactive fullerene-based (C_{60}−Pd) polymer and HiPCO single-wall carbon nanotubes, which were noncovalently modified by 1-pyrenebutiric acid (pyr-SWCNTs), were electrochemically prepared under multiscan cyclic voltammetry conditions. With respect to blank polymer, superior conductive, capacitive, and viscoelasitic properties of the composite were demonstrated. Composition of pyr-SWCNTs was determined by thermogravimetric analyses, which showed one molecule of 1-pyrenebutiric acid per ∼20 carbon atoms of SWCNT. Atomic force microscopy imaging revealed that pyr-SWCNTs form tangles of pyr-SWCNTs bundles surrounded by globular clusters of the C_{60}−Pd polymer. Peaks characteristic of both pyr-SWCNTs (radial breathing modes at ∼200 to 300 cm^{-1}) and C_{60}−Pd polymer in the Raman spectra recorded for the composite confirmed the presence of pyr-SWCNTs in the composite film. The mass of the deposited film was in situ measured by piezoelectric microgravimetry with the use of an electrochemical quartz crystal microbalance (EQCM). Then, curves of the current, resonant frequency change, and dynamic resistance change versus the potential in different potential ranges were simultaneously recorded in a blank acetonitrile solution of tetrabutylammonium perchlorate. Specific capacitance, determined at −1.20 V for the composite as 90 F g^{-1}, was twice as high as that for the polymer. Electrochemical impedance spectroscopy was used to determine impedance parameters of both the C_{60}−Pd polymer and C_{60}−Pd/pyr-SWCNTs composite film. This data analysis indicated increased capacitance and decreased resistance for the new composite film.

Introduction

Carbon nanotubes (CNTs), built of cylindrical seamless "welded" graphene sheets with nanometer-range diameter, exhibit outstanding physical and chemical properties, including relatively high electrical conductivity, impressive chemical stability, low density, large surface area, and exceptional mechanical modulus and strength.[1] In electrochemistry, they have attracted attention as a new anode material for Li^+ ion batteries,[2−4] capacitors,[5−7] and electrochemical actuators[8,9] and sensors.[10] CNTs have also been examined as new hydrogen storage materials for hydrogen/air fuel cells.[11−13] Moreover, they were tested as attractive novel electrode materials, showing the ability to mediate electron transfer of electroactive species in solution.[14−17]

Two types of CNTs can be distinguished with respect to their structure, that is, single-wall (SWCNTs) and multiwall (MWCNTs) carbon nanotubes.[18] SWCNTs are formed from a single graphene sheet rolled into a cylinder with a diameter in the range of 1−5 nm and a length of several micrometers. MWCNTs consist of graphene sheets rolled into closed coaxial cylinders.

For many practical applications, CNTs are immobilized on solid supports. They can be confined, for instance, to electrodes, by either direct growth,[19,20] manual manipulation,[21] or random spreading.[22] This surface immobilization can also be accomplished by integration of CNTs into more complex assemblies.[23,24] A common procedure of incorporating CNTs into assemblies is through chemical functionalization of the nanotube surface, which enables covalent bonding to the surface functional group of the support material.[25−28]

Particularly interesting are recent intensively studied composites of conducting polymers and CNTs.[29−50] The incorporation of CNTs into conducting polymers leads to changes of both their electrical and mechanical properties. That is, conductivity as well as stability of the resulting composites is often increased, as compared to those of genuine polymers. Moreover, the presence of CNTs can significantly increase electrical capacitance of the conducting polymers. Recently, different procedures were proposed to fabricate composites of conducting polymers and CNTs. The most common one, adopted for conducting polymers soluble in organic solvents, is a drop-coating procedure. It consists in dispensing a drop of the polymer solution containing suspended CNTs on the electrode surface and, then, allowing the solvent to evaporate.[29−38] Several composites, like poly(3-hexylthiophene)/MWCNTs,[29] poly(3-octylthiophene)/SWCNTs,[30,31] poly(1,4-phenylenevinylene)/ MWCNTs,[32] and

* To whom correspondence should be addressed. E-mail: wkutner@ichf.edu.pl. Phone: +48 22 343 32 17. Fax: +48 22 343 33 33 (W.K.); E-mail: Francis.DSouza@wichita.edu. Phone: +1 316-978-7380. Fax: +1 316-978-3431 (F.D.S).
[†] Polish Academy of Sciences.
[‡] University of Bialystok.
[§] Warsaw University of Technology.
[||] Wichita State University.
[⊥] Cardinal Stefan Wyszynski University.

10.1021/jp810173c CCC: $40.75
Published on Web 04/01/2009

copoly(phenylenevinylene)/SWCNTs,[33−38] were prepared that way. In these composites, CNTs are dispersed randomly in the polymeric material. A similar procedure was used to prepare composites from stable suspensions of conducting polymers and CNTs.[39] In the case of polymers that are insoluble in common organic solvents, such as polypyrrole or polyaniline, composites of these polymers and CNTs were prepared in situ, that is, in the course of chemical[40−46] or electrochemical[40,47−53] polymerization carried out in solutions containing suspended CNTs and dissolved respective monomers. The structure and properties of these composites depend upon the morphology of the CNT film initially deposited on the electrode surface. For a charge storage application, the drop-coating procedure was used to immobilize CNTs on a solid conducting substrate. Next, the porous film of CNTs was coated by a conducting polymer film. In another approach, CNTs were directly grown onto the electrode surface. This procedure enables one to control both orientation and order of this component in the composite material.[44,49,50]

Recent investigations of optical, electrical, and mechanical properties imply that the CNTs containing composite materials are promising for various applications. For instance, composites of CNTs and conducting materials were tested for electrochemical storage of energy.[40−42,52−54] The presence of CNTs in a polymeric film on the electrode results in the increase of capacitance of the electrode, higher mechanical strength of the film, and its improved stability. Conductivity of these composites is higher than that of individual components. Moreover, these composites can be used to fabricate optoelectronic devices. For instance, photovoltaic devices were fabricated from the poly(3-octylthiophene)/MWCNT[32] and poly(3-octylthiophene)/SWCNTs[30] composites. The poly(3,4-ethylenedioxythiophene)/SWCNT composite was applied for constructing the hole-conducting films in organic light-emitting diodes.[39] The polypyrrole/SWCNT composite was used to fabricate field emitters.[51] Furthermore, these composites are promising for sensing applications. For example, the polypyrrole/SWCNT composite was used for fabrication of an amperometric glucose biosensor.[55]

Recently, a lot of attention has been focused on the development of novel electroactive polymers based on fullerenes.[56−63] One of our approaches involves two-component films of polymers of fullerenes or their derivatives and transition-metal complexes, C_{60}−M, formed on the electrode surface during electroreduction carried out in solutions containing fullerenes and complexes of such transition metals as palladium,[59−62] rhodium,[59] iridium,[59] or platinum.[63] In the resulting films, the fullerene moieties are most likely bound to the metal centers in an η^2 fashion to form a polymeric network. In contrast to most conducting polymers, C_{60}−M polymers exhibit electrochemical activity in the negative potential range due to electroreduction and electrooxidation of the fullerene moieties present. Recently, it was shown that the C_{60}−Pd polymer coated electrode exhibited a very high capacitance, which was potential controlled.[64]

It is reasonable to integrate the C_{60}−M polymer and SWCNTs to come up with a composite film challenging novel applications, especially those related to its conducting and electrochemical redox properties. This goal has partially been achieved in the present study,[65] in which the formation and selected features of a composite of the C_{60}−Pd polymer and SWCNTs noncovalently surface functionalized by 1-pyrenbutiric acid, pyr-SWCNTs, are reported.

Experimental Section

Chemicals. C_{60} (99.5% purity) was from M. E. R. Corp. (Tucson, AZ, U.S.A.) or SES Research (Houston, TX, U.S.A.). HiPCO single-wall carbon nanotubes were from Carbon Nanotechnology, Inc. (Houston, TX, U.S.A.), and 1-pyrenebutiric acid was from Aldrich. Palladium(II) acetate, $Pd(ac)_2$, (98% purity) was from Aldrich. The toluene (anhydrous, 99.8%) and dimethylformamide (anhydrous, 99.8%) were from Aldrich, and the acetonitrile (puriss, absolute) and 1,2-dichlorobenzene (anhydrous, 99%) were from Fluka; the solvents were used as received. The tetra(*n*-butyl)ammonium hexafluorophosphate, $(TBA)PF_6$, (puriss, electrochemical grade, 99.0%) and tetra(*n*-butyl)ammonium perchlorate, $(TBA)ClO_4$, supporting electrolyte salts from Fluka were used as received.

Apparatus and Procedures. A 160 W ultrasonic bath type IS-3R of InterSonic (Olsztyn, Poland) was used for dissolution of C_{60} and dispersion of pyr-SWCNTs in selected electrolyte solutions.

Simultaneous cyclic voltammetry (cv) and piezoelectric microgravimetriy (pm) experiments were performed by using potentiostat type EP-21 of Elpan (Lubawa, Poland) connected to the electrochemical quartz crystal microbalance type EQCM 5710 of the Institute of Physical Chemistry (Warsaw, Poland) under the EQCM 5710-S2 software control. This microbalance allowed for simultaneous measurement of changes of current, resonant frequency, and dynamic resistance of a 10 MHz At-cut quartz crystal resonator during potential scanning. The resonators featured 5 mm diameter Au film circular electrodes.

An AUTOLAB computerized electrochemistry system of Eco Chemie (Utrecht, The Netherlands) was used for the cv and electrochemical impedance spectroscopy (eis) measurements on the film-coated electrodes. This system was equipped with the expansion cards of the PGSTAT 12 potentiostat and the FRA frequency response analyzer, and controlled by the GPES 4.9 software of Eco Chemie. A conventional three-neck V-shaped glass electrochemical minicell of the working solution with a volume of less than 0.5 mL was used for cv experiments in the three-electrode system. A 1 mm diameter Pt disk, Pt coil, and Ag|AgCl served as the working, auxiliary, and reference electrode, respectively. The eis measurements were carried out for the frequency range of 10 kHz to 0.1 Hz at various constant electrode potentials using a 10 mV sine wave amplitude for all experiments. The polymer- or composite-film-modified electrode was kept at the selected potential for ~120 s before performing the eis measurements. Data were collected and analyzed using Zplot version 2.9c software for Windows of Scribner Associates, Inc. (Southern Pines, NC, U.S.A.).

Atomic force microscopy (AFM) imaging was performed with a Nanoscope III instrument of the Digital Instruments/Veeco Metrology Group.

The Raman spectra were recorded with the use of the Almega Raman spectrometer of Nicolet (Madison, WI, U.S.A.) equipped with a confocal Raman microscope. The spectra were recorded, with 2 cm^{-1} resolution, by using an excitation laser beam of 780 nm wavelength at 25 °C.

Thermogravimetric analysis (tga) was performed with the TGA 951 thermogravimetric analyzer controlled by the Thermal Analyst 2100 of DuPont. The 1.5−1.8 mg samples were placed in an aluminum pan. The samples were heated from 25 to 1050 °C in air with the rate of 10 °C min^{-1}.

All experiments were performed at ambient temperature, (20 ± 1) °C, if not stated otherwise.

Preparation of pyr-SWCNTs. Single-wall carbon nanotubes were noncovalently surface modified with 1-pyrenebutiric acid

using a procedure similar to that reported earlier for preparation of the pyr-SWCNTs bearing receptor sites.[66,67] That is, a 1.5 mg sample of purified HiPCO carbon nanotubes was added to a 3.2 mg sample of 1-pyrenebutyric acid dissolved in a 15 mL sample of dry DMF, and the reaction mixture was stirred for 48 h at room temperature. The resulting mixture was sonicated for 6 h at 20 °C followed by centrifugation for 2 h. The excess of 1-pyrenebutiric acid was removed by separating the centrifugate from the black solid precipitate. This precipitate was further purified by dissolving it in a 5 mL sample of fresh DMF, sonicating for 30 min at 20 °C, followed by centrifugation for 1 h. Then, the nonadsorbed pyrene reagent was removed by separating the centrifugate from the black precipitate. This process was repeated (at least twice). At the end, a 10 mL sample of fresh DMF was added to the resulting solid, and the mixture was sonicated for 15 min at 20 °C. The obtained uniform black suspension, stable at room temperature for weeks, was used for preparation of the composite films.

Preparation of the C_{60}−Pd/pyr-SWCNTs Composite. Both the C_{60}−Pd polymer film and the C_{60}−Pd/pyr-SWCNTs composite film were grown from the 0.1 M $(TBA)ClO_4$ solution of toluene/acetonitrile (4:1, *v*/*v*) containing C_{60} and $Pd(ac)_2$ in the absence and presence of pyr-SWCNTs, respectively, under multiscan cv conditions between −0.2 and −1.05 V at the potential sweep rate of 0.1 V s^{-1}. pyr-SWCNTs tend to aggregate and slowly form sediment in the solution containing a supporting electrolyte salt, like $(TBA)PF_6$ or $(TBA)ClO_4$. Therefore, the working electrode used for preparation of the composite was kept horizontally, facing up, in order to allow for pyr-SWCNTs to descend onto its surface and thus incorporate into the polymer matrix during electropolymerization of C_{60}. Once the film had been formed, the modified electrode was rinsed with the toluene/acetonitrile (4:1, *v*/*v*) mixed solvent solution. Then, the film-coated electrode was placed in a 0.1 M solution of the chosen supporting electrolyte in acetonitrile, and the cv, pm, and eis measurements were performed to study its electrical and viscoelastic properties.

Results and Discussion

First, thermogravimetric determination of the pyr-SWCNTs composition was performed in order to estimate the extent of the surface functionalization of SWCNTs. Next, both the C_{60}−Pd polymer and C_{60}−Pd/pyr-SWCNTs composite films were prepared under cv conditions, and their electrochemical properties were unraveled. For the same preparation procedure, both films were deposited on the ITO electrodes and imaged by AFM. Raman spectroscopy investigations were then performed in order to confirm the presence of pyr-SWCNTs in the composite film. Subsequently, simultaneous measurements of the pm and cv behavior of the C_{60}−Pd polymer film and the C_{60}−Pd/pyr-SWCNTs composite film were carried out with the use of EQCM in order to compare capacitive, resistive, and viscoelastic properties of both films. Eventually, electrical parameters, such as capacitance, ion diffusion resistance, and charge-transfer resistance of the investigated thin-film-coated electrodes were determined at different potentials by eis studies.

Determination of the pyr-SWCNTs Composition by Thermogravimetric Analysis. 1-Pyrenebutiric acid and its derivatives were successfully used for noncovalent functionalization of CNT side walls.[68] The tga measurements of pyr-SWCNTs allowed estimation of the extent of noncovalent surface functionalization of SWCNTs with 1-pyrenebutiric acid. Curves of relative mass versus temperature for genuine SWCNTs, 1-pyrenebutiric acid, and pyr-SWCNTs are shown as curves 1, 2, and 3, respectively, in Figure 1. The sample of genuine SWCNTs is stable without significant mass loss below ∼350 °C (curve 1 in Figure 1). Above this temperature, however, SWCNTs decompose in one step as the mass abruptly decreases with the increase of temperature. However, 1-pyrenebutiric acid decomposes in two steps, that is, at ∼275 and 375 °C (curve 2 in Figure 1). In curve 3 in Figure 1 for pyr-SWCNTs, there are features resembling those appearing in curves 1 and 2 in Figure 1. That is, there are three pronounced mass loss steps. The first step, that is, that at ∼275 °C, can be assigned to the removal of 1-pyrenebutiric acid from the SWCNT surface and its decomposition. The second step at ∼400 °C is attributed to decomposition of SWCNTs. The mass loss of the pyr-SWCNTs sample was about 44.5 and 45.5% in the lower- and higher-temperature range, respectively. These values indicate that one molecule of 1-pyrenebutiric acid corresponds to ∼20 carbon atoms of SWCNT. That is, most of the available SWCNT surface has been coated by closely packed, and π-stacked with the SWCNT sidewall, 1-pyrenebutiric acid molecules, similarly as in the case described in the literature.[68]

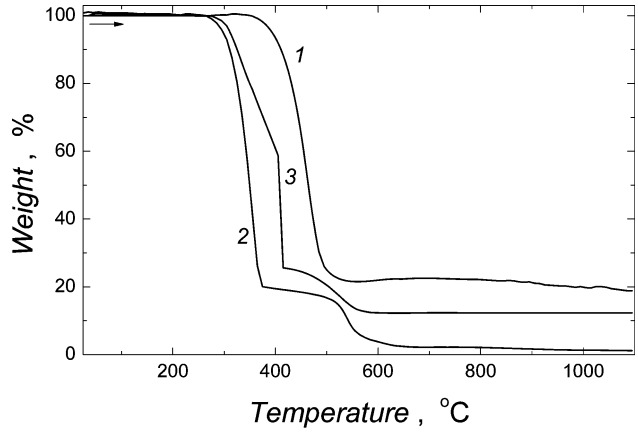

Figure 1. Thermogravimetry curves for (1) SWCNTs, (2) 1-pyrenebutiric acid, and (3) SWCNTs noncovalently modified by 1-pyrenebutiric acid, pyr-SWCNTs; heating rate 10 °C min^{-1}, air atmosphere.

Cyclic Voltammetric Electrodeposition and Selected Property Studies of the C_{60}−Pd Polymer Film and C_{60}−Pd/pyr-SWCNTs Composite Film. Electrochemical reduction of C_{60} in the 0.1 M $(TBA)ClO_4$ toluene/acetonitrile (4:1, *v*/*v*) mixed solvent solution, in the presence of $Pd(ac)_2$, leads to deposition of an electrochemically active, black film on the electrode. Figure 2 shows multiscan cyclic voltammograms for the formation of a C_{60}−Pd polymer film (Figure 2a) and a C_{60}−Pd/pyr-SWCNTs composite film (Figure 2b). The former film was deposited from the solution, which was 2.5 mM in $Pd(ac)_2$ and 0.34 mM in C_{60}. The latter film was prepared under the same solution conditions, except in the presence of pyr-SWCNTs. The increase in current with the increase of the cv cycle number and corresponding growth of the black deposit indicates deposition of the film. After transfer to a blank 0.1 M $(TBA)ClO_4$ acetonitrile solution, both modified electrodes were electrochemically active in the potential range of −0.50 to −1.50 V (Figure 3). However, cathodic and anodic currents for the C_{60}−Pd/pyr-SWCNTs film (curve 1 in Figure 3a) were much higher than those for the C_{60}−Pd polymer film (curve 2 in Figure 3a). These different currents may imply that higher capacitance and lower resistance characterize the electrode coated by the C_{60}−Pd polymer film doped with pyr-SWCNTs. From the highest slopes of tangents of the rising portions of the cathodic currents in the potential range of ∼−0.45 to −0.65 V, apparent redox conductivity values were determined as 2.9×10^{-6} and

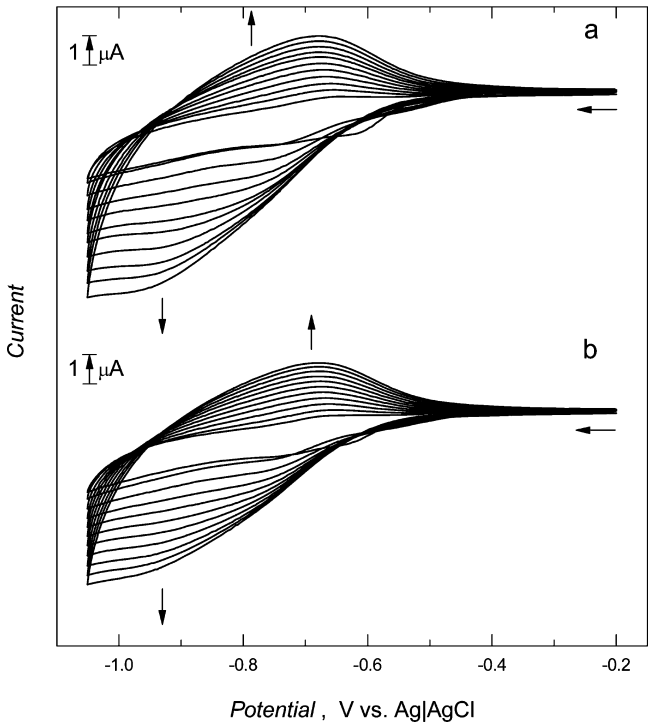

Figure 2. Multiscan cyclic voltammograms for electrodeposition of films of (a) C_{60}−Pd polymer and (b) C_{60}−Pd/pyr-SWCNTs composite in solutions of (a) 0.34 mM C_{60} and 2.5 mM palladium(II) acetate and (b) 0.34 mM C_{60}, 2.5 mM palladium(II) acetate, and pyr-SWCNTs, in toluene/acetonitrile (4:1, *v*/*v*) on the 0.1 mm diameter Pt disk electrode. The potential sweep rate was 100 mV/s.

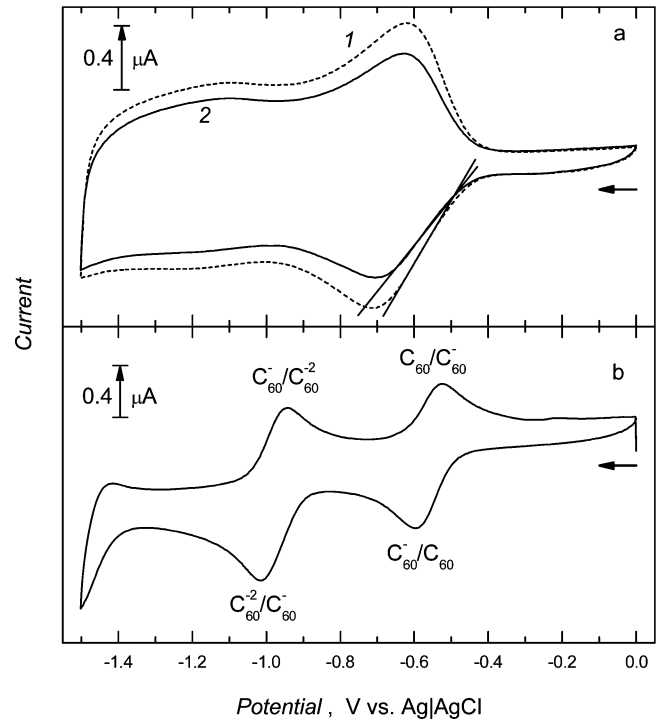

Figure 3. Cyclic voltammograms for films of (a) a C_{60}Pd/pyr-SWCNTs composite, curve 1, and a C_{60}−Pd polymer, curve 2, as well as (b) 0.34 mM C_{60} in 0.1 M (TBA)ClO_4, in 1,2-dichlorobenzene. Film (1) was deposited from a solution of pyr-SWCNTs, 0.34 mM C_{60}, 2.5 mM $Pd(ac)_2$, and 0.1 M (TBA)PF_6 in toluene/acetonitrile (4:1, *v*/*v*). Film (2) was deposited from solution of 0.34 mM C_{60}, 2.5 mM $Pd(ac)_2$, and 0.1 M (TBA)PF_6, in toluene/acetonitrile (4:1, *v*/*v*). The potential sweep rate was 100 mV/s.

3.7×10^{-6} S for the film of the C_{60}−Pd polymer and the C_{60}−Pd/pyr-SWCNTs composite, respectively. Notably, the redox conductivity of the C_{60}−Pd polymer film doped with pyr-SWCNTs is higher than that of the undoped C_{60}−Pd polymer film. This effect may be attributed to the changes in structure and porosity of the film. It was shown[60] that C_{60}−Pd electroreduction is associated with the transport of cations from the solution into the solid phase of polymer. Easier penetration of the C_{60}−Pd/pyr-SWCNTs composite by counterions results in higher redox conductivity in comparison to that of the C_{60}−Pd polymer.

Atomic Force Microscopy Investigations of the Surface of the C_{60}−Pd Polymer Film and C_{60}−Pd/pyr-SWCNTs Composite Film. The AFM imaging of surfaces of the C_{60}−Pd polymer film and C_{60}−Pd/pyr-SWCNTs composite film prepared under cv conditions (14 cv cycles, 0.1 V s^{-1}) on the ITO electrodes provided information on the surface topography of the films and the film thickness.

Both films were electrodeposited from 0.34 mM C_{60}, 2.5 mM $Pd(ac)_2$, and 0.1 M (TBA)PF_6 in toluene/acetonitrile (4:1, *v*/*v*) in the absence and presence of pyr-SWCNTs for a film of the C_{60}−Pd polymer and composite film, respectively.

Figure 4a shows the AFM image of the C_{60}−Pd polymer film deposited on ITO. This film is relatively uniform and built of microscopically distinguishable globular clusters with 180−220 nm diameters. Those clusters are merged together forming a ∼100 nm thick film that coats the entire surface of the ITO electrode.

The AFM image in Figure 4b shows surface of the C_{60}−Pd/pyr-SWCNTs composite film deposited on the ITO electrode. The topography of this film is quite different than that of the C_{60}−Pd polymer film. That is, a tangle of bundles of pyr-SWCNTs coated by the 90−100 nm diameter globules of the C_{60}−Pd polymer are seen. The average thickness of this film is ∼120 nm.

Surface roughness, $R_{sa} = A_{3D}/A_{2D}$, represented by the ratio of area in three-dimensional space, A_{3D}, to that projected into two-dimensional space, A_{2D}, of the C_{60}−Pd/pyr-SWCNTs composite, determined as 1.72, is higher than that of the C_{60}−Pd polymer, determined as 1.37. These results confirm the conclusion that the redox conductivity of the composite is higher than that of the polymer due to changes in the morphology of the film.

Raman Spectroscopy Investigations of the C_{60}−Pd Polymer Film and C_{60}−Pd/pyr-SWCNTs Composite Film. Raman spectroscopy is a powerful tool for probing the local environment of both the C_{60} molecules and SWCNTs.[69] Herein, it is used to prove the formation of the C_{60}−Pd/pyr-SWCNTs composite (Figure 5). The Raman spectrum for pristine C_{60} (not shown) exhibits 10 lines of active, that is, 8 H_g and 2 A_g, intramolecular vibrations.[69] In the course of C_{60} electropolymerization, new intermolecular bonds between the C_{60} cages and the $Pd(ac)_2$ spacer molecules are formed, which are accompanied by changes in the intramolecular C−C bonding. This inter- and intramolecular bond formation results in breaking the I_h symmetry of C_{60} and induces splitting and shifting of 10 modes characteristic for pristine C_{60}. Therefore, the Raman spectrum for the C_{60}−Pd polymer film (Figure 5a) contains many more details than that for the pristine C_{60} film, confirming the polymer film formation on the electrode surface. The Raman spectrum for pristine pyr-SWCNTs (Figure 5b) consists of two main characteristic groups of vibrations, that is, radial breathing modes, RBMs, in the range of 100−250 cm^{-1} as well as the D and the G modes at around 1290 and 1590 cm^{-1}, respectively.[70] In the Raman spectrum for the C_{60}−Pd/pyr-SWCNTs composite film (Figure 5c), there are peaks characteristic of both C_{60}−Pd and pyr-SWCNTs. All of these peaks are expected for pyr-

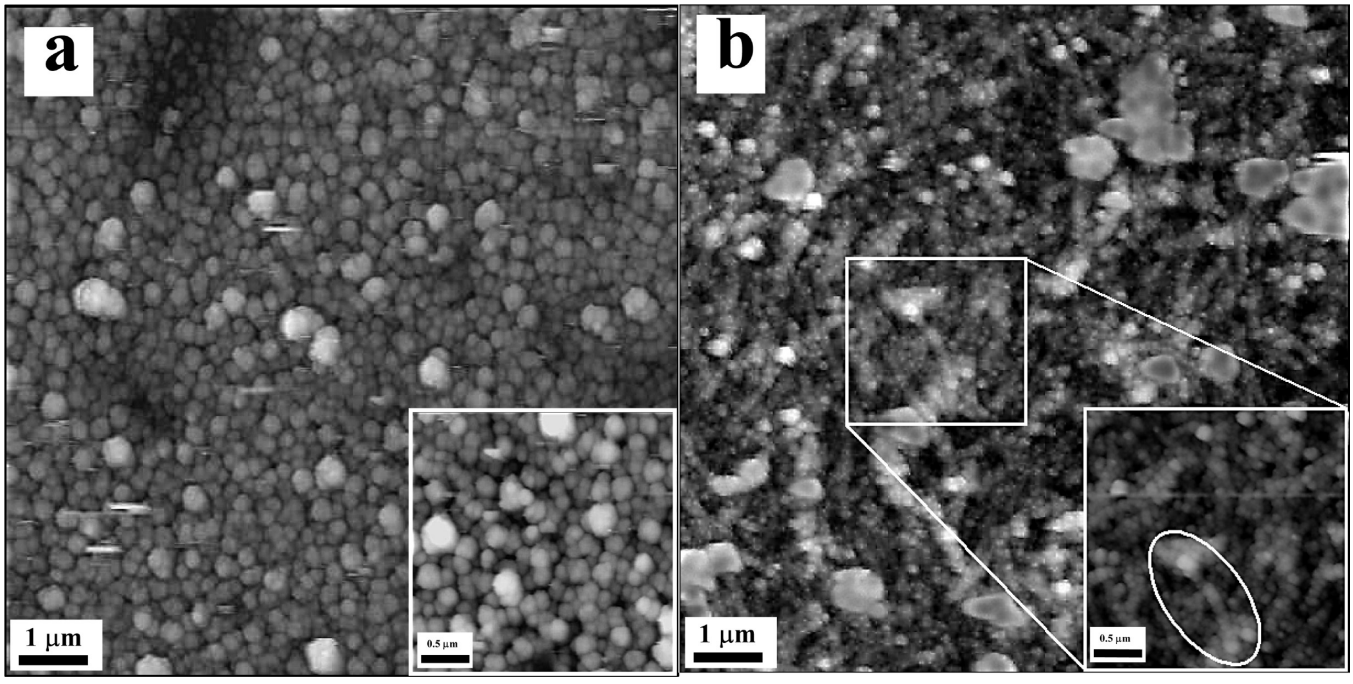

Figure 4. Atomic force microscopic images at 10 × 10 μm^2 magnification of (a) the film of the C_{60}−Pd polymer and (b) the film of the C_{60}−Pd/pyr-SWCNTs composite electrochemically deposited on the ITO electrode. Insets show images at 3.5 × 3.5 μm^2 magnification. Film (a) was deposited from a solution of 0.34 mM C_{60}, 2.5 mM $Pd(ac)_2$, and 0.1 M $(TBA)PF_6$ in toluene/acetonitrile (4:1, *v*/*v*). Film (b) was deposited from a solution of pyr-SWCNTs, 0.34 mM C_{60}, 2.5 mM $Pd(ac)_2$, and 0.1 M $(TBA)PF_6$, in toluene/acetonitrile (4:1, *v*/*v*). The potential sweep rate was 100 mV/s, and the number of cv scans was 14.

SWCNTs incorporated into the film during electropolymerization of C_{60}−Pd, as is seen in the superimposed spectrum for C_{60}−Pd and pyr-SWCNTs (Figure 5d). There are no differences in the intensity and Raman shift in the D and G mode for pristine pyr-SWCNTs (Figure 5b) and pyr-SWCNTs in the composite (Figure 5c). The D bands correspond to disordered structures in carbon nanotubes. The same intensity of the D modes suggests that the polymer grains sticking to side walls of pyr-SWCNTs do not alter the defect density in pyr-SWCNTs.[71] However, the RBM peaks for the pyr-SWCNTs film are deconvoluted in the spectrum for C_{60}−Pd/pyr-SWCNTs (Figure 5c). A very strong Raman peak at ∼266−268 cm^{-1} is observed for both pristine pyr-SWCNTs (Figure 5b) and pyr-SWCNTs in the composite (Figure 5c). This peak is characteristic for highly bundled HiPCO SWCNT samples with Raman excitation at 785 nm.[72] The second RBM peak at ∼228 cm^{-1} observed for the pristine pyr-SWCNTs (Figure 5b) is split into two peaks at 228 and 208 cm^{-1} for pyr-SWCNTs in the composite (Figure 5c). Moreover, the intensity of these new peaks is lower than that for pristine pyr-SWCNTs. This intensity change may be due to either interactions of the SWCNT with neighboring C_{60}−Pd[73] or a higher extent of aggregation of pyr-SWCNTs.[72]

Simultaneous Piezoelectric Microgravimetry and Cyclic Voltammetry Behavior of the C_{60}−Pd Polymer Film and the C_{60}−Pd/pyr-SWCNTs Composite Film. Simultaneously measured with EQCM multiscan cv curves, resonant frequency changes versus potential and dynamic resistance changes versus potential, which led to electropolymeric deposition of the C_{60}−Pd polymer film and the C_{60}−Pd/pyr-SWCNTs composite film on the quartz resonators, are presented in Figure 6. The film deposition was manifested by the decrease of the resonant frequency, Δf_{total}, with the increase of the cv cycle number (curves 2 and 2′ in Figure 6a and b). The deposition was carried out to reach the same value of the total frequency decrease. The total frequency shift due to mass loading of the quartz

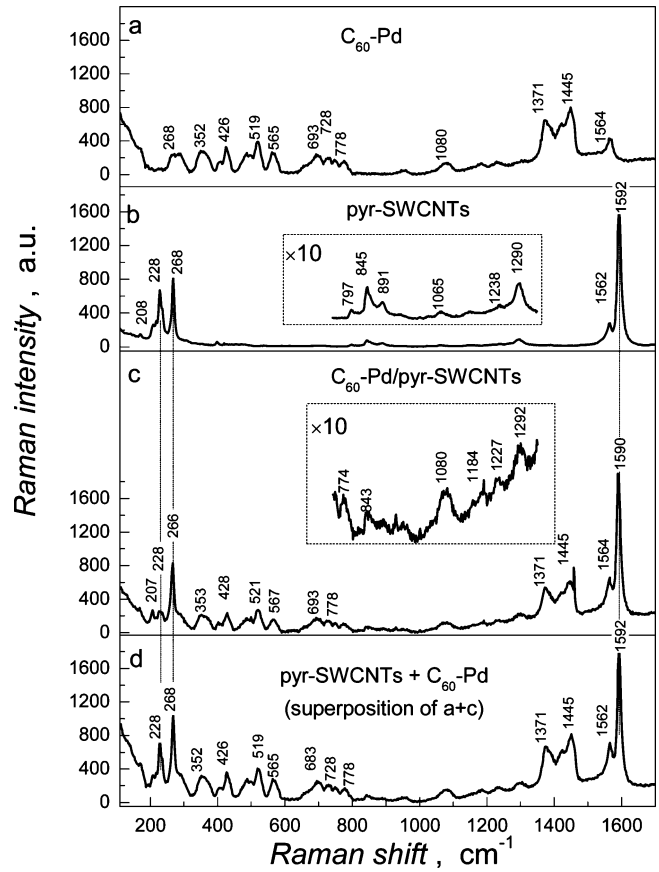

Figure 5. Raman spectra for (a) the film of the C_{60}−Pd polymer, (b) the film of pyr-SWCNTs drop-coated from the $CHCl_3$ solution, (c) the film of the C_{60}−Pd/pyr-SWCNTs composite [(b) and (c) were deposited by electrochemical polymerization from the 0.1 M $(TBA)ClO_4$, in 1,2-dichlorobenzene solution], and (d) superposition of the spectra (a) and (b).

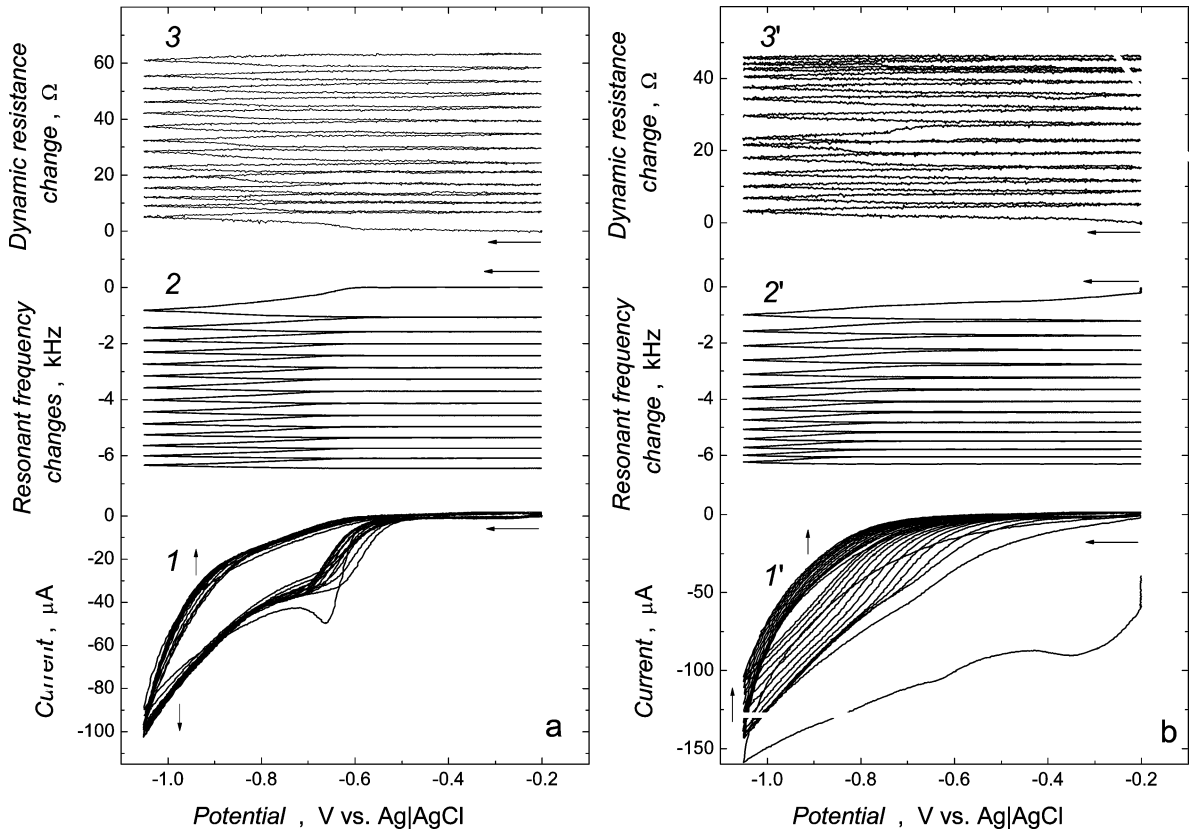

Figure 6. Curves of (1 and 1′) multiscan cyclic voltammetry, (2 and 2′) resonant frequency changes, and (3 and 3′) dynamic resistance changes for electrodeposition of films of (a) a C_{60}−Pd polymer and (b) the C_{60}−Pd/pyr-SWCNT composite in a mixed C_{60}, pyr-SWCNTs, and palladium(II) acetate solution of acetonitrile/toluene (1:4, *v*/*v*) on the Au film electrode of the 10 MHz quartz resonator. The potential sweep rate was 100 mV/s.

resonator immersed in a viscous medium is caused both by the changes of its mass, Δf_{mass}, and by the changes of the viscoelastic properties of a contacting medium, Δf_{vis}[74]

$$\Delta f_{total} = \Delta f_{mass} + \Delta f_{vis} = -\frac{2f_0^2 \Delta m}{A(\mu_Q \rho_Q)^{0.5}} + (-f_0^{1.5})\left(\frac{\eta_L \rho_L}{\pi \mu_Q \rho_Q}\right)^{0.5} \quad (1)$$

where $\mu_Q = 2.947 \times 10^{11}$ (g cm^{-1} s^{-2}) is the shear modulus of quartz, $\rho_Q = 2.648$ g cm^{-3} is the quartz density, η_L (g cm^{-1} s^{-1}) and ρ_L (g cm^{-3}) is the dynamic viscosity and density, respectively, of the contacting liquid, A (cm^2) is the acoustically active area of the quartz resonator, and f_0 (Hz) is the fundamental frequency of the quartz resonator. Qualitatively, the considerations involving the quartz resonator in contact with viscous liquid can be extended to viscous film coats. Therefore, simultaneous measurement of a variable related to viscoelasticity of a system, like dynamic resistance of the quartz resonator, R,[74] is necessary to determine the contribution to the total frequency change originating from the viscoelasticity change

$$R = \frac{A}{k^2}(2\pi f_0 \eta_L \rho_L)^{0.5} \quad (2)$$

where $k^2 = 7.74 \times 10^{-3}$ (A^2 s^2 cm^{-2}) is the electromechanical coupling factor for the quartz resonator. Hence, from the second part of eq 1 and eq 2, it follows that the frequency change due to the viscosity change is opposite to the dynamic resistance

$$\Delta f_{vis} = -\frac{k^2 R f_0}{\pi A(2\mu_Q \rho_Q)^{0.5}} \quad (3)$$

The Δf_{total} for the C_{60}−Pd polymer film and C_{60}−Pd/pyr-SWCNTs composite film, measured after 14 cv cycles, was ∼6437 and 6295 Hz, respectively (curve 2 and 2′ in Figure 6a and b, respectively). However, electropolymerization of C_{60}−Pd in the presence of pyr-SWCNTs resulted in smaller changes in the dynamic resistance than those corresponding to the deposition of the polymer alone, indicating smaller changes with potential in the film rigity. Presumably, the presence of pyr-SWCNTs in the composite was responsible for this effect. On the basis of eq 3, Δf_{vis} for the C_{60}−Pd polymer film and the C_{60}−Pd/pyr-SWCNTs composite film was calculated to be 6.3 and 4.6 Hz, respectively. These changes are very small compared to those of Δf_{total}. It means that during deposition, the film coating the resonator surface is rigid and does not significantly influence the total frequency shift. After subtraction of Δf_{vis} from Δf_{total}, on the basis of the first part of eq 1, the mass of the deposited films was calculated. The mass of the C_{60}−Pd polymer film and C_{60}−Pd/pyr-SWCNTs composite film, deposited after 14 cv cycles (Figure 6a and b), was 5.58 and 5.46 μg, respectively.

The quartz resonators, with their electrodes coated either by the C_{60}−Pd polymer film or the C_{60}−Pd/pyr-SWCNTs composite film, were transferred to the blank 0.1 M (TBA)PF_6

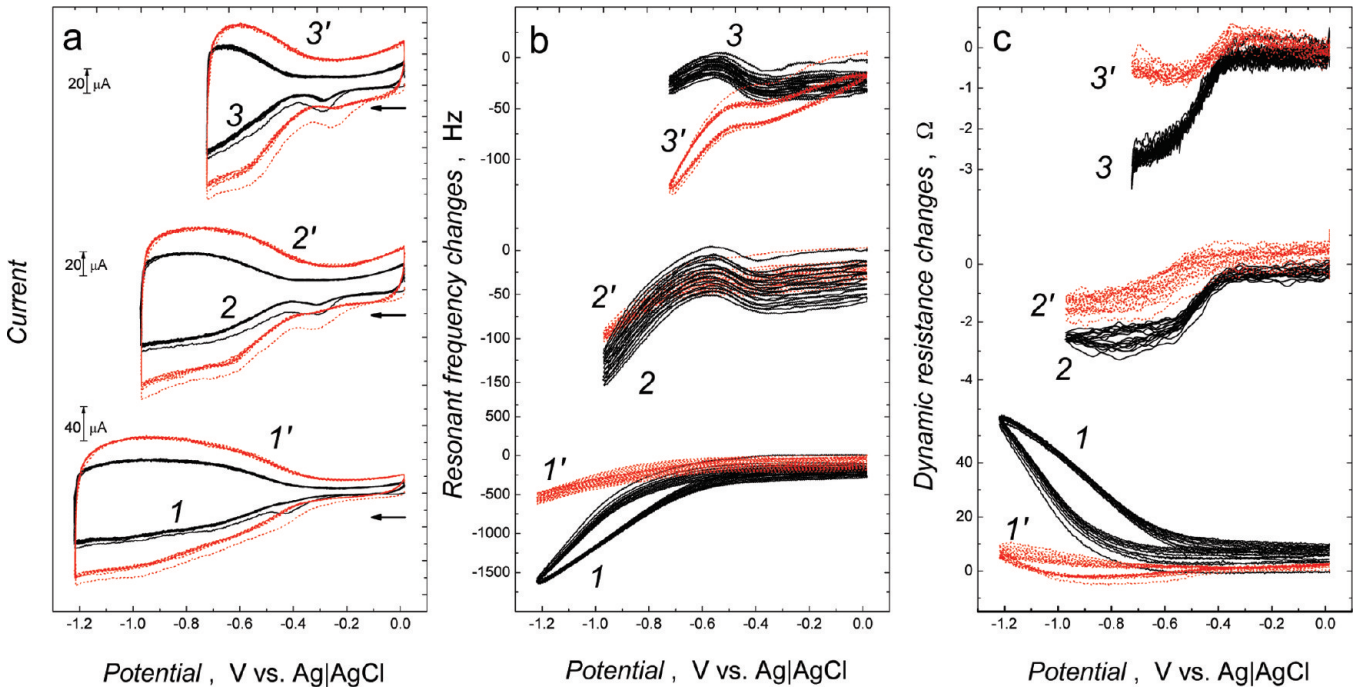

Figure 7. Curves for different cathodic reversal potentials for (a) multiscan cyclic voltammetry, (b) resonance frequency changes, and (c) dynamic resistance changes for the films of the C_{60}−Pd polymer (black solid curves 1, 2, and 3) and C_{60}−Pd/pyr-SWCNTs composite (red short dash curves 1′, 2′, and 3′) in 0.1 M (TBA)PF_6 in acetonitrile. The potential sweep rate was 50 mV/s, and a Au film of the 10 MHz quartz resonator served as the working electrode.

acetonitrile solutions, and curves of the current, resonant frequency changes, and dynamic resistance changes versus potential were simultaneously recorded for different cathodic potential reversals (Figure 7). Each film was electrochemically active at potentials more negative than ∼−0.40 V. For these potentials, both cathodic and anodic currents for the C_{60}−Pd/pyr-SWCNTs composite film were almost twice as high as those for the C_{60}−Pd polymer film (Figure 7a). These higher currents for the composite film are due to higher capacitance of the composite-film-coated electrode (see the next section). The pronounced differences in the resonant frequency and dynamic resistance for the C_{60}−Pd polymer and C_{60}−Pd/pyr-SWCNTs composite films are seen in Figure 7b and c, respectively, for potentials more negative than −0.90 V. That is, when the negatively scanned potential reaches −0.90 V, the frequency rapidly decreases, and dynamic resistance increases. However, for the C_{60}−Pd/pyr-SWCNTs film, this frequency decrease is three times smaller than that for the C_{60}−Pd film, as seen in curves 1 and 1′ in Figure 7b. Changes in the dynamic resistance for the C_{60}−Pd film are three times larger than those for the C_{60}−Pd/pyr-SWCNTs film (curves 1 and 1′ in Figure 7c). This behavior suggests that the C_{60}−Pd/pyr-SWCNTs film is more rigid than the C_{60}−Pd film for potentials more negative than −0.90 V.

Electrochemical Impedance Spectroscopy Studies of the C_{60}−Pd Polymer Film and C_{60}−Pd/pyr-SWCNTs Composite Film. The eis technique is often used to study electrical properties of the film-coated electrodes into more detail.[75−82] The eis measurements, performed in the present work to investigate impedance properties of both the C_{60}−Pd polymer- and C_{60}−Pd/pyr-SWCNTs composite-film-coated electrodes, covered both the semi-infinite and finite (very low frequency) regime of counterion diffusion, allowing for determination of electrical parameters, such as low-frequency redox capacitance, charge-transfer resistance, ion diffusion resistance, and double-layer capacitance of the thin-film-coated electrodes.

SCHEME 1: Equivalent Circuit of the Electrode−Film−Solution Interface[a]

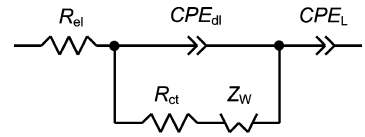

[a] R_{el} is the ohmic resistance related to the ionic conductivity of the electrolyte, R_{ct} is the total charge-transfer resistance of the faradaic process, Z_w is the impedance due to the ion diffusion in the film, CPE_{dl} represents an experimental double-layer capacitance of the film|electrolyte interface, and CPE_L represents an experimental limiting capacitance arising from the finite thickness of the film.

An electric equivalent circuit for modeling the film-coated electrode should include elements reflecting electrochemical processes at the electrode|C_{60}−Pd polymer|electrolyte or electrode|C_{60}−Pd polymer|pyr-SWCNTs|(electrolyte solution) interface. For instance, an equivalent circuit depicted in Scheme 1 represents these interfaces well.[83] It served this purpose well also in studies performed by others, but it certainly should not be considered as unique. In the present work, experimental data on the dependence of the real part of the impedance (Z') versus the imaginary part of the impedance (Z'') at different potentials (Figures 8 and 9) were simulated, and the equivalent circuit parameters were fitted. The resulting electrical parameters are plotted versus the potential in Figure 10. The complex plane impedance, so-called Nyquist, plots (Z' versus $-Z''$) for the electrode coated by the C_{60}−Pd film and C_{60}−Pd/pyr-SWCNTs film in 0.1 M (TBA)ClO_4, in acetonitrile, for different potential-governed C_{60} redox states are shown in Figures 8 and 9, respectively. Figures 8a and 9a show the Nyquist plots for films of the polymer- and composite-coated electrode, respectively, for the potential range of 0 to −0.30 V, and Figures 8b and 9b show that for the same films for potentials between −0.40 and −1.10 V.

For the potential range of 0 to −0.30 V, the C_{60}−Pd film is, for all intents and purposes, nonconductive, and impedance

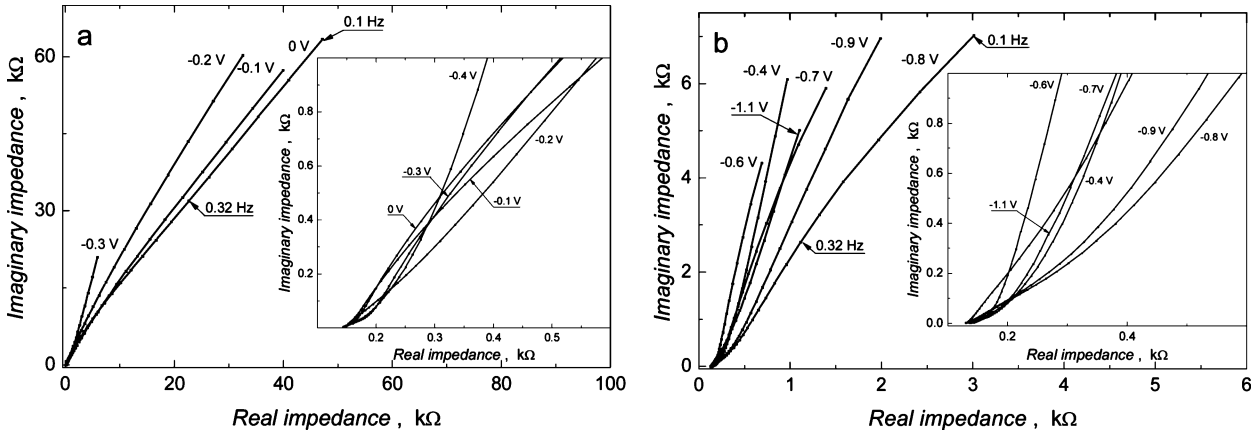

Figure 8. Complex plane impedance plots for the C_{60}−Pd polymer-film-coated electrode in 0.1 M $(TBA)ClO_4$, in acetonitrile, in the potential range of (a) 0 to −0.30 V and (b) −0.40 to −1.10 V. The C_{60}−Pd polymer film was grown under cv conditions in 0.1 M $(TBA)ClO_4$, 0.27 mM C_{60}, and 3.65 mM $Pd(ac)_2$ in toluene/acetonitrile (4:1, *v*/*v*).

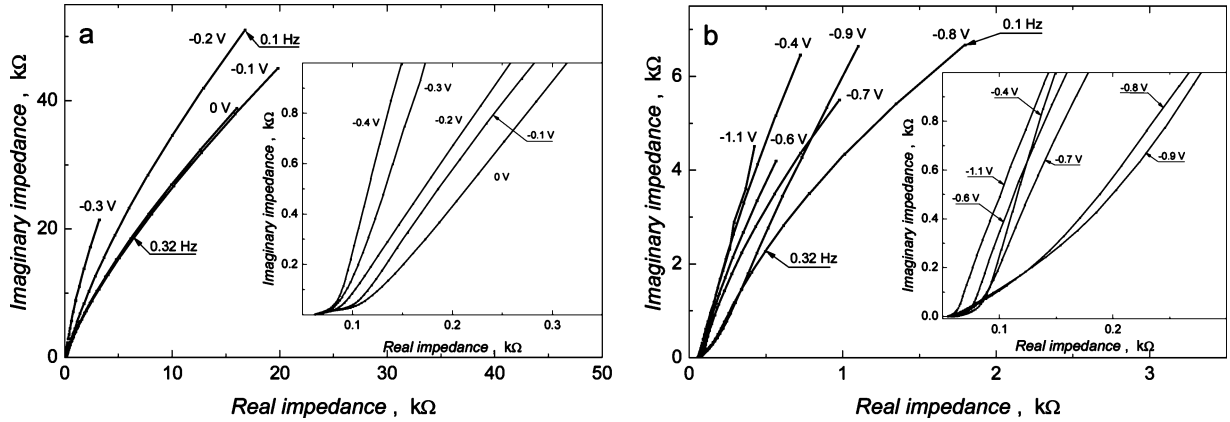

Figure 9. Complex plane impedance plots for the C_{60}−Pd/pyr-SWCNTs composite-film-coated electrode in 0.1 M $(TBA)ClO_4$, in acetonitrile, in the potential range of (a) 0 to −0.30 V and (b) −0.40 to −1.10 V. The C_{60}−Pd/pyr-SWCNTs composite film was grown under cv conditions in 0.1 M $(TBA)ClO_4$, 0.27 mM C_{60}, and 3.65 mM $Pd(ac)_2$ in toluene/acetonitrile (4:1, *v*/*v*) in the presence of pyr-SWCNTs.

diagrams for the electrode coated with this polymer show a large semicircle due to the high charge-transfer resistance (Figure 8a). That is, both the Z' and $-Z''$ values dramatically increase with the frequency decrease. An electric equivalent circuit represents the charging of the double layer of the polymer|solution interface, which consists of the connected in series ohmic resistance related to the ionic conductivity of the electrolyte, R_{el}, the double-layer capacitance of the film|electrolyte interface, CPE_{dl}, and the in-series connected capacitance, also referred to as the low-frequency redox capacitance, arising from the finite thickness of the film, CPE_L. For this potential region, the values of both the low-frequency redox capacitance and the double-layer capacitance are low and approximately constant (curves 1, 1′ and 4, 4′ in Figure 10a and d, respectively). The behavior of the C_{60}−Pd/pyr-SWCNTs composite-modified electrode is different than that of the polymer-coated electrode. That is, the Z' versus $-Z''$ data are arranged along a straight line with the $\pi/4$ slope for high frequency (inset in Figure 9a). Presumably, this behavior suggests that the presence of pyr-SWCNTs in the film facilitates the counteranion diffusion inside of the film, even for the potential range, in which the polymer is not conductive. The behavior of the low-frequancy redox capacitance and double-layer capacitance is similar to that for the polymer-coated electrode (curves 1′ and 4′ in Figure 10a and d, respectively).

At the potential close to −0.40 V, electroreduction of the C_{60}−Pd film begins. The Z' versus $-Z''$ curve (inset in Figure 7a) approximates the response of the finite transmission line with the $\pi/4$ slope of a nearly linear segment of the plot (Warburg-type region) at high frequency, giving rise to an almost vertical linear segment at low frequency. In case of the C_{60}−Pd/pyr-SWCNTs composite-film-coated electrode, such a behavior is recorded even for potentials less negative than −0.40 V (inset in Figure 9a).

For the −0.40 to −0.60 V potential range, the observed current increase on the cv curve may be attributed to both faradaic and nonfaradaic processes (Figure 3a). Both the real and imaginary components of the impedance at low frequencies are low. For modified electrodes, redox capacitance (Figure 10a) and double-layer capacitance (Figure 10d) increases as the charge-transfer resistance (Figure 10b) and ion diffusion resistance (Figure 10c) decrease. This behavior is due to the increase of the extent of both the C_{60} electroreduction and electronic conductivity of the film.

For the potential range of −0.60 to −0.90 V, no current peak is seen on the cv curve for C_{60} in solution (Figure 3b). It means that the entire amount of C_{60} is electroreduced to the monoanion (C_{60}^-), and hence, the polymer shows no redox conductivity (Figures 8b and 9b and their insets). The redox capacitance is slightly lower (curves 1 and 1′ in Figure 10a), while the charge-transfer resistance (curves 2 and 2′ in Figure 10b) and ion diffusion resistance are higher (curves 3 and 3′ in Figure 10c) for both films. However, changes in both resistances are more dramatic for the polymer- than those for the composite-modified electrode (Figure 10c). Apparently, the presence of pyr-SWCNTs in the film increases its conductivity (Figure 10b and c). The double-layer capacitance remains unchanged for the

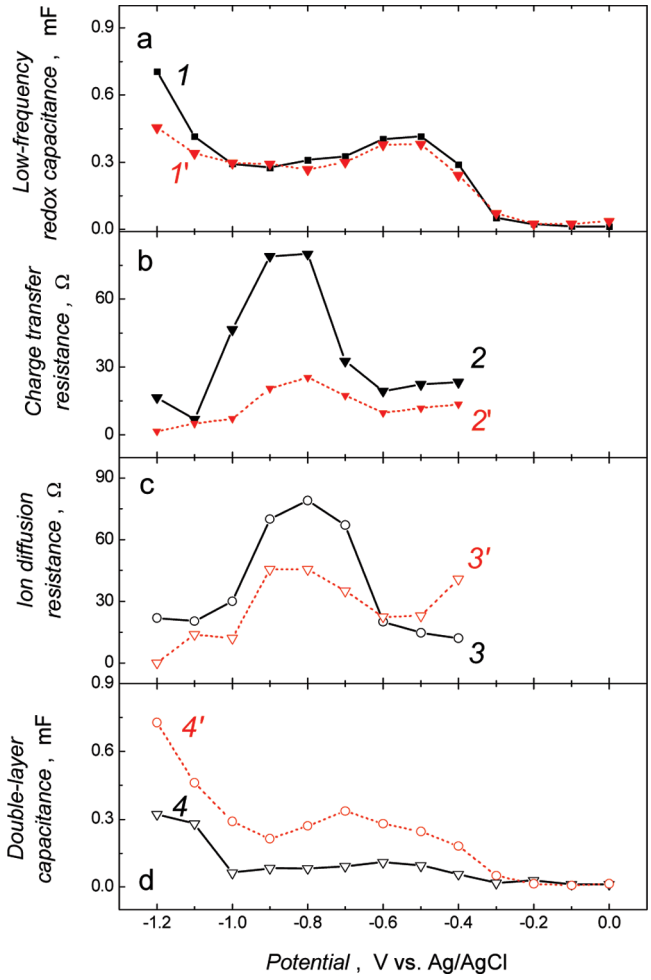

Figure 10. Curves of (a) the low-frequency redox capacitance change, (b) the charge-transfer resistance change, (c) the ion diffusion resistance change, and (d) the double-layer capacitance change versus potential for the films of the C_{60}−Pd polymer (curves 1−4) and the C_{60}−Pd/pyr-SWCNTs composite (curves 1′−4′) in 0.1 M $(TBA)ClO_4$ in acetonitrile.

C_{60}−Pd-coated electrode (curve 4 in Figure 10d), while it is increased for the C_{60}−Pd/pyr-SWCNTs film (curves 4′ in Figure 10d).

When the potential reaches the value of the second cathodic cv peak potential of one-electron reduction of C_{60}^{-}/C_{60}^{2-} (radical monoanion), that is, that which is more negative than −0.90 V (Figure 3b), both the real and imaginary components of the impedance decrease again with the increase of the applied potential (Figures 8b and 9b). Both the redox capacitance (curves 1 and 1′ in Figure 10a) and the double-layer capacitance (curves 4 and 4′ in Figure 10d) increase, while the charge-transfer resistance (curves 2 and 2′ in Figure 10b) and ion diffusion resistance (curves 3 and 3′ in Figure 10c) decrease.

Conclusions

Cyclic voltammetry electroreduction of C_{60} in the presence of $Pd(ac)_2$ and pyr-SWCNTs results in the formation of a composite film of the fullerene polymer and pyr-SWCNTs on the electrode surface. This composite is built of a tangle of bundles of pyr-SWCNTs coated by the 90−100 nm diameter globules of the C_{60}−Pd polymer. The presence of pyr-SWCNTs in the film markedly increases the capacitance and decreases the resistance of the electrode. Importantly, the behavior of electrical parameters, such as the low-frequency redox capacitance, charge-transfer resistance, ion diffusion resistance, and double-layer capacitance of both thin-film-coated electrodes, is associated with the redox-conductive character of the C_{60}−Pd polymer. Although the electrochemical behavior and viscoelasticity of the C_{60}−Pd and C_{60}−Pd/pyr-SWCNTs films are almost the same for potentials more positive than −0.90 V, the C_{60} Pd/pyr-SWCNTs film is more rigid and stable than the pristine C_{60}−Pd film for potentials more negative than −0.90 V. Further studies using a newly devised composite electroactive material for electrocatalytic and sensor applications[10] are in progress in our laboratories.

Acknowledgment. Dr. E. Utzig is gratefully acknowledged for her help in the tga measurements. This work was financially supported by the National Science Foundation (Grant 0804015 to F.D.) and the Ministry of Science and Higher Education of Poland (Project No. N204 046 31/1214 to W.K. and N204 3747 33 to K.W.). F.D. is also thankful to the Royal Society of Chemistry for an International Author Travel Award.

Note Added after ASAP Publication. This article posted ASAP on April 1, 2009. Several errors were corrected throughout the paper. The final correct version posted April 10, 2009.

References and Notes

(1) Ebbesen, W. *Carbon Nanotubes, Preparation and Properties*; CRC Press: Boca Raton, FL, 1997.
(2) Claye, A. S.; Fisher, J. E.; Huffman, C. B.; Rinzler, A. G.; Smalley, R. E. *J. Electrochem. Soc.* **2000**, *147*, 2845.
(3) Honda, K.; Yoshimura, M.; Kawakita, K.; Fujishima, A.; Sakamoto, Y.; Yasui, K.; Nishio, N.; Matsuda, H. *J. Electrochem. Soc.* **2004**, *151*, A532.
(4) Wu, C. T.; Wang, C. S.; Zhang, X. B.; Yang, H. S.; Qi, Z. F.; He, P. M.; Li, W. Z. *J. Electrochem. Soc.* **1999**, *146*, 1696.
(5) An, K. H.; Kim, W. S.; Park, Y. S.; Moon, J. M.; Bae, D. J.; Lim, S. C.; Lee, Y. S.; Lee, Y. H. *Adv. Funct. Mater.* **2001**, *11*, 387.
(6) Niu, C.; Sichel, E. K.; Hoch, R.; Moy, D.; Tennent, H. *Appl. Phys. Lett.* **1997**, *70*, 1480.
(7) Liu, C.; Bard, A. J.; Wudl, F.; Weitz, I.; Heath, J. R. *Electrochem. Solid State Lett.* **1999**, *2*, 577.
(8) Baughman, R. H.; Cui, C.; Zakhidov, A. A.; Iqbal, Z.; Barisci, J. N.; Spinks, G. M.; Wallace, G. G.; Mazzoldi, A.; Rossi, D. D.; Rinzler, A.; Jaschinski, O.; Roth, S.; Kertesz, M. *Science* **1999**, *284*, 1340.
(9) Spinks, G. M.; Wallace, G. G.; Baughman, R. H.; Dai, L. *Electroactive Polymer Actuators as Artificial Muscles*; Bar-Cohen Y., Ed.; SPIE Press: Washington, DC, 2001.
(10) Sherigara, B. S.; Kutner, W.; D'Souza, F. *Electroanalysis* **2003**, *15*, 753.
(11) Qin, X.; Gao, X. P.; Liu, H.; Yuan, H. T.; Gong, W. L.; Song, D. Y. *Electrochem. Solid State Lett.* **2000**, *3*, 532.
(12) Lombardi, I.; Bestetti, M.; Mazzocchia, C.; Cavallotti, P. L.; Ducati, U. *Electrochem. Solid State Lett.* **2004**, *7*, A115.
(13) Nutzenadel, C.; Zuttel, A.; Chartouni, D.; Schlapbach, L. *Electrochem. Solid State Lett.* **1999**, *2*, 30.
(14) Wang, G.; Liu, X.; Yu, B.; Luo, G. *J. Electroanal. Chem.* **2004**, *567*, 227.
(15) Davis, J. J.; Coles, R. J.; Hill, H. A. *J. Electroanal. Chem.* **1997**, *440*, 279.
(16) Wang, J.; Li, M.; Shi, Z.; Li, N.; Gu, Z. *Anal. Chem.* **2002**, *74*, 1993.
(17) Wang, J.; Musameh, M.; Lin, Y. *J. Am. Chem. Soc.* **2003**, *125*, 2408.
(18) Saito, R.; Dresselhaus, G.; Dresselhaus, M. S. *Physical Properties of Carbon Nanotubes*; Imperial College Press: London, 1998.
(19) Qi, P.; Vermesh, O.; Grecu, M.; Javey, A.; Wang, Q.; Dai, H. *Nano Lett.* **2003**, *82*, 961.
(20) Valentini, L.; Armentano, I.; Kenny, J. M.; Cantalini, C.; Lozzi, L.; Santuccci, S. *Appl. Phys. Lett.* **2003**, *82*, 961.
(21) Rueckes, T.; Kim, K.; Joselevich, E.; Tseng, G. Y.; Cheung, C.; Lieber, C. M. *Science* **2000**, *289*, 94.
(22) Martel, R.; Schmidt, T.; Shea, H. R.; Hertel, T.; Avouris, P. *Appl. Phys. Lett.* **1998**, *73*, 2447.
(23) Kong, J.; Franklin, N. R.; Zhou, C.; Chaplin, M. G.; Peng, S.; Cho, K.; Dai, H. *Science* **2000**, *287*, 622.

(24) Tans, S. J.; Verschueren; Dekkker, C. *Nature (London)* **1998**, *393*, 49.
(25) Bahr, J. L.; Tour, J. M. *Mater. Chem.* **2002**, *12*, 1952.
(26) Sinott, S. B. *J. Nanosci. Nanotechnol.* **2002**, *2*, 113.
(27) Stevens, J. L.; Huang, A. Y.; Peng, H. Q.; Chiang, L. W.; Khabashesku, V. N.; Margrave, J. L. *Nano Lett.* **2003**, *3*, 331.
(28) Ramanathan, T.; Fisher, F. T.; Ruoff, R. S.; Brinson, L. C. *Chem. Mater.* **2005**, *17*, 1290.
(29) Lee, S. B.; Katayama, T.; Kajii, H.; Araki, H.; Yoshino, K. *Synth. Met.* **2001**, *121*, 1591.
(30) Kumakis, E.; Amaratunga, G. A. J. *Appl. Phys. Lett.* **2002**, *80*, 112.
(31) Musa, I.; Baxendale, M.; Amaratunga, G. A. J.; Eccleston, W. *Synth. Met.* **1999**, *102*, 1250.
(32) Ago, H.; Petritsch, K.; Shaffer, M. S.; Windle, A. H.; Friend, R. H. *Adv. Mater.* **1999**, *11*, 1281.
(33) Coleman, J. N.; Curran, S.; Dalton, A. B.; Davey, A. P.; McCarthy, B.; Blau, W. J.; Barklie, R. C. *Synth. Met.* **1999**, *102*, 1174.
(34) Dalton, A. B.; Blau, W. J.; Chambers, G.; Coleman, J. N.; Henderson, K.; Lefrant, S.; McCarthy, B.; Stephan, C.; Byrne, H. J. *Synth. Met.* **2001**, *121*, 1217.
(35) McCarthy, B.; Coleman, J. N.; Czerw, J. N.; Dalton, A. B.; Byrne, H. J.; Takleab, D.; Iyer, P.; Ajayan, P. M.; Blau, W. J.; Carroll, D. L. *Nanotechnology* **2001**, *12*, 187.
(36) McCarthy, B.; Coleman, J. N.; Czerw, J. N.; Dalton, A. B.; Carroll, D. L.; Blau, W. J. *Synth. Met.* **2001**, *121*, 1225.
(37) Curran, S. A.; Ajayan, P. M.; Blau, P. M.; Carroll, D. L.; Coleman, J. N.; Coleman, J. N.; Davey, A. P.; Drury, A.; McCarthy, B.; Mayer, S.; Strevens, A. *Adv. Mater.* **1998**, *10*, 1091.
(38) Coleman, J. N.; O'Brien, D. F.; Panhuis, M. I. H.; Dalton, A. B.; McCarthy, B.; Barklie, R. C.; Blau, W. J. *Synth. Met.* **2001**, *121*, 1229.
(39) Woo, H. S.; Czerw, R.; Webster, S.; Carroll, D. L.; Park, J. W.; Lee, J. H. *Synth. Met.* **2001**, *116*, 369.
(40) Jurewicz, K.; Depeux, S.; Bertagna, V.; Beguin, F.; Frackowiak, E. *Chem. Phys. Lett.* **2001**, *347*, 36.
(41) Frackowiak, E.; Khomenko, V.; Jurewicz, K.; Lota, K.; Beguin, F. *J. Power Sources.* **2006**, *153*, 413.
(42) Xiao, Q.; Zhou, X. *Electrochim. Acta* **2003**, *48*, 575.
(43) Fan, J.; Wan, M.; Zhu, D.; Chang, B.; Pan, Z.; Xie, S. *Synth. Met.* **1999**, *102*, 1266.
(44) Feng, W.; Bai, X. D.; Liang, Y. Q.; Wang, X. G.; Ioshino, K. *Carbon* **2003**, *41*, 1551.
(45) Valter, B.; Ram, M. K.; Nicolini, C. *Langmuir* **2003**, *18*, 1535.
(46) An, K. H.; Jeon, K. K.; Neo, J. K.; Lim, S. C.; Bae, D. J.; Lee, Y. H. *J. Electrochem. Soc.* **2003**, *150*, A1058.
(47) Huang, J. E.; Li, X. H.; Xu, J. C.; Li, H. L. *Carbon* **2003**, *41*, 2731.
(48) Hassanien, A.; Gao, M.; Tokumoto, M.; Dai, L. *Chem. Phys. Lett.* **2001**, *342*, 479.
(49) Chen, J. H.; Huang, Z. P.; Wang, D. Z.; Yang, S. X.; Li, W. Z.; Wen, J. G.; Ren, Z. F. *Synth. Met.* **2002**, *125*, 289.
(50) Chen, J. H.; Huang, Z. P.; Wang, D. Z.; Yang, S. X.; Wen, J. G.; Ren, Z. F. *Appl. Phys. A* **2001**, *73*, 129.
(51) Jin, Y. W.; Jung, J. E.; Park, Y. J.; Choi, J. H.; Jung, D. S.; Lee, H. W.; Park, S. H.; Lee, N. S.; Kim, J. M.; Ko, T. Y.; Lee, S. J.; Hwang, S. Y.; You, J. H.; Yoo, J. B.; Park, C. Y. *J. Appl. Phys.* **2002**, *92*, 1065.
(52) Hughes, M.; G.Z, C.; Shaffer, M. S. P.; Fray, D. J.; Windle, A. H. *Chem. Mater.* **2002**, *14*, 1610.
(53) Ovsyannikova, E. V.; Efimov, O. N.; Moravsky, A. P.; Loufty, R. O.; Krinichnaya, E. P.; Alpatova, N. M. *Russ. J. Electrochem.* **2005**, *41*, 439.
(54) Frackowiak, E.; Beguin, F. *Carbon* **2002**, *40*, 1775.
(55) Callegari, A.; Cosnier, S.; Marcaccio, M.; Paolucci, D.; Paolucci, F.; Georgakilas, V.; Tagmataarchis, N.; Vazquez, E.; Prato, M. *J. Mater. Chem.* **2004**, *14*, 807.
(56) Fedurco, M.; Costa, D. A.; Balch, A. L.; Fawcett, W. R. *Angew. Chem., Int. Ed. Engl.* **1995**, *34*, 194.
(57) Winkler, K.; Costa, D. A.; Balch, A. L.; Fawcett, W. R. *J. Phys. Chem.* **1995**, *99*, 17431.
(58) Krinichnaya, E. P.; Moravsky, A. P.; Efimov, O.; Sobczak, J. W.; Winkler, K.; Kutner, W.; Balch, A. L. *J. Mater. Chem.* **2005**, *15*, 1468.
(59) Balch, A. L.; Costa, D. A.; Winkler, K. *J. Am. Chem. Soc.* **1998**, *120*, 9614.
(60) Winkler, K.; Bettencourt-Dias, A. d.; Balch, A. L. *Chem. Mater.* **1999**, *11*, 2265.
(61) Winkler, K.; Bettencourt-Dias, A. d.; Balch, A. L. *Chem. Mater.* **2000**, *12*, 1386.
(62) Winkler, K.; Noworyta, K.; Kutner, W.; Balch, A. L. *J. Electrochem. Soc.* **2000**, *147*, 2597.
(63) Hayashi, A.; Bettencourt-Dias, A. d.; Winkler, K.; Balch, A. L. *J. Mater. Chem.* **2002**, *12*, 2116.
(64) Winkler, K.; Grodzka, E.; D'Souza, F.; Balch, A. L. *J. Electrochem. Soc.* **2007**, *154*, K1.
(65) Pieta, P.; Grodzka, E.; Winkler, K.; Venukadasula, G. M.; D'Souza, F.; Kutner, W. *Phys. Status Solidi B* **2008**, *245*, 2292.
(66) D'Souza, F.; Chitta, R.; Sandanayaka, A. S. D.; Subbaiya, N. K.; D'Souza, L.; Araki, Y.; Ito, O. *Chem.—Eur. J.* **2007**, *13*, 8277.
(67) D'Souza, F.; Chitta, R.; Sandanayaka, A. S. D.; Subbaiyan, N. K.; D'Souza, L.; Araki, Y.; Ito, O. *J. Am. Chem. Soc.* **2007**, *129*, 15865.
(68) Chen, R. J.; Zhang, Y.; Wang, D.; Dai, H. *J. Am. Chem. Soc.* **2001**, *123*, 3838.
(69) Dresselhaus, M. S.; Dresselhaus, G.; Eklund, P. C. *Science of Fullerenes and Carbon Nanotubes*. *Vibrational Modes*; Academic Press, Inc.: San Diago, CA, 1996; p 329.
(70) Rao, A. M.; Richter, E.; Bandow, S.; Chase, B.; Eklund, P. C.; Williams, K. A.; Fang, S.; Subbaswamy, K. R.; Menon, M.; Thess, A.; Smalley, R. E.; Dresselhaus, G.; Dresselhaus, M. S. *Science* **1997**, *275*, 187.
(71) Zhang, R.; Wang, X. *Chem. Mater.* **2007**, *17*, 976.
(72) Heller, D. A.; Barone, P. W.; Swanson, J. P.; Mayrhofer, R. M.; Strano, M. S. *J. Phys. Chem. B* **2004**, *108*, 6905.
(73) Fantini, C.; Usrey, M. L.; Strano, M. S. *J. Phys. Chem. C* **2007**, *111*, 17941.
(74) Thompson, M.; Kipling, A. L.; Duncan-Hewitt, W. C.; Rajaković, L. V.; Ćavić-Vlasak, B. A. *Analyst* **1991**, *116*, 881.
(75) Duffitt, G. L.; Pickup, P. G. *J. Chem. Soc., Faraday Trans.* **1992**, *88*, 1417.
(76) Komura, T.; Sakabayashi, H.; Takahashi, K. *Bull. Chem. Soc. Jpn.* **1995**, *68*, 476.
(77) Osaka, T.; Nakajima, T.; Shiota, K.; Momma, T. *J. Electrochem. Soc.* **1991**, *138*, 2853.
(78) Pickup, P. G. *J. Chem. Soc., Faraday Trans.* **1990**, *86*, 3631.
(79) Ren, X.; Pickup, P. G. *J. Phys. Chem.* **1993**, *97*, 5356.
(80) Ren, X.; Pickup, P. G. *J. Electrochem. Soc.* **1992**, *139*, 2097.
(81) Ren, X.; Pickup, P. G. *J. Chem. Soc., Faraday Trans.* **1993**, *89*, 321.
(82) Rubinstein, I.; Rishpon, J.; Gottesfeld, S. *J. Electrochem. Soc.* **1986**, *133*, 729.
(83) Gao, Z.; Kvarnström, C.; Ivaska, A. *Electrochim. Acta* **1994**, *39*.

JP810173C